Additive Manufacturing 26 (2019) 242–249

Contents lists available at ScienceDirect

Additive Manufacturing

journal homepage: www.elsevier.com/locate/addma

Full Length Article

Improvement in build-direction thermal conductivity in extrusion-based polymer additive manufacturing through thermal annealing

Hardikkumar Prajapati, Divya Chalise, Darshan Ravoori, Robert M. Taylor, Ankur Jain*

Mechanical and Aerospace Engineering Department, University of Texas at Arlington, Arlington, TX, USA

ARTICLE INFO

Keywords:
Polymer extrusion additive manufacturing
Thermal annealing
Thermal conductivity enhancement
Filament adhesion

ABSTRACT

While additive manufacturing offers significant advantages compared to traditional manufacturing technologies, deterioration in thermal and mechanical properties compared to properties of the underlying materials is a serious concern. In the context of polymer extrusion based additive manufacturing, post-process approaches, such as thermal annealing have been reported for improving mechanical properties based on reptation of polymer chains and enhanced filament-to-filament adhesion. However, there is a lack of similar work for improving thermal properties such as thermal conductivity. This paper reports significant enhancement in build-direction thermal conductivity of polymer extrusion based parts as a result of thermal annealing. Over 150% improvement is observed when annealed at 135 °C for 96 h. The effect of annealing temperature and time on thermal conductivity enhancement is investigated through experiments. A theoretical model based on Arrhenius kinetics for neck growth and a heat transfer model for the consequent impact on inter-layer thermal contact resistance is developed. Predicted thermal conductivity enhancement is found to be in good agreement with experimental data for a wide range of annealing temperature and time. The theoretical model may play a key role in developing practical thermal annealing strategies that account for the multiple constraints involved in annealing of polymer parts. This work may facilitate the use of polymer extrusion additive manufacturing for producing enhanced thermal conductivity parts capable of withstanding thermal loads.

1. Introduction

Polymer based additive manufacturing (AM) processes [1,2] have been widely investigated for a variety of applications. In a polymer extrusion based AM process, a polymer wire is heated to above its glass transition temperature and selectively extruded on to a bed through a rastering nozzle [3,4]. Extruded filaments merge into each other while cooling down, which results in the final part. Extrusion AM processes typically use materials such as acrylonitrile butadiene styrene (ABS), ULTEM, and other amorphous thermoplastics due to the wide range of temperatures in which they exhibit glassy, viscous behavior that allows them to be softened, deposited and bonded during layered printing processes.

While additive manufacturing offers the capability to manufacture parts that are difficult or impossible through traditional manufacturing methods and a significantly expanded design space, additively manufactured parts often suffer from poor mechanical and thermal properties compared to the properties of the underlying materials. Several papers have reported reduced mechanical properties [5–8], showing lower modulus, strength, toughness, and strong anisotropy in parts built using polymer extrusion AM. This is usually due to incomplete merging between adjacent lines in the build plane or in the build direction due to unoptimized process parameters. An understanding of process-structure-property relationships as well as post-process strategies for improving thermal and mechanical properties is therefore essential.

Multiple studies have reported measurement of mechanical properties as a function of process parameters. Material continuity within a part is developed as contour beads are deposited in adjacent roads and bonding takes place via diffusion welding. Consequently, part stiffness and strength strongly depend on the quality of the developed inter-bead bond strength, contact area, gaps and voids, as well as bead shape and orientation with respect to loading direction. Due to the inherently directional nature of the process, anisotropic mechanical behavior of additively manufactured polymer parts has been reported for a variety of properties, such as tensile and compressive strength [8,9], fatigue strength [10,11], flexural strength [12], etc. Most papers in this direction report strong dependence of the nature of anisotropy on process parameters such as raster speed and orientation, layer thickness, infill percentage, etc.

Similarly, thermal conductivity has been shown through

* Corresponding author at: 500 W First St, Rm 211, Arlington, TX, 76019, USA.
E-mail address: jaina@uta.edu (A. Jain).

https://doi.org/10.1016/j.addma.2019.01.004
Received 26 October 2018; Received in revised form 5 January 2019; Accepted 22 January 2019
Available online 31 January 2019
2214-8604/

measurements to be lower than the inherent thermal conductivity of the filament material [13] and to be a function of various process parameters [14,15]. Thermal conductivity in the build direction has been shown to be significantly lower than in the raster direction. The reduced thermal conductivity and anisotropy have been explained on the basis of incomplete merging and significant thermal contact resistance between layers resulting from imperfect contact [13]. The reduced thermal conductivity in the build direction may be a cause of concern for applications where the part is expected to withstand heat loads, since thermal conductivity is the key property governing the rate of flow of heat.

It is clearly important to develop strategies to improve and repair thermal conductivity, particularly in the build direction. To a limited extent, this could be done by choosing the optimal process parameters [14,15]. However, this approach has practical limitations based on the range in which these process parameters can be varied and their impact on throughput. For example, it has been shown that thermal conductivity of a polymer extrusion based part is higher for lower extrusion speed [14,15], however, this is undesirable as it reduces throughput.

Post-process thermal annealing is a possible approach for improving thermal properties of additively manufactured parts. Thermal annealing is commonly used for improving grain structure in traditionally manufactured metal parts through exposure to high temperature for a period of time [16]. Thermal annealing has also been used to a limited extent for modifying the microstructure of parts manufactured using polymer AM, with the motivation of improving mechanical properties [17]. Significant increase in fracture toughness has been reported for 3D printed ABS parts that are isothermally annealed at temperatures of 125 °C, 135 °C, and 175 °C for times between 2 and 168 h [17]. The physical mechanisms and models for healing at thermoplastic interfaces via thermal treatment have been documented in the literature [18,19]. Improved filament-to-filament adhesion is known to occur through sintering and reptation across bead interfaces [20,21]. Similar to mechanical strength, thermal conductivity is also a strong function of the contact area and quality of bonding between filaments. Therefore, the mechanisms of reptation-based enhancement in filament-to-filament adhesion due to thermal annealing might improve thermal conductivity, similar to reported improvement in mechanical properties [17]. However, there is a lack of work on the effect of annealing on thermal conductivity, and theoretical modeling to predict the extent of thermal conductivity enhancement as a function of annealing parameters. Some work has been reported on measurement of neck size as a function of annealing temperature and time [22], and theoretical modeling of the neck growth process [23]. However, there is a lack of work on connecting these processes to thermal properties of the built part.

This paper presents experimental and theoretical analysis of post-process thermal annealing for improving build-direction thermal conductivity in additively manufactured parts. Post-process exposure of polymer extrusion built parts to different temperatures for different times, followed by measurement of build-direction thermal conductivity is carried out. Significant enhancement in thermal conductivity is reported as a result of annealing. For example, around 150% improvement is reported for annealing at 135 °C for 96 h, which increases thermal conductivity of the part to nearly the value for the underlying material. A theoretical model based on a power-law Arrhenius relationship between annealing parameters and inter-layer neck size, and a thermal conduction based relationship between thermal contact resistance and neck size is proposed. Theoretical predictions are found to be in good agreement with direct experimental measurements. The design space of thermal annealing parameters is explored using this theoretical model, highlighting several interesting trade-offs and important considerations in designing a robust thermal annealing strategy. Experimental data on the effect of annealing on thermal properties and the theoretical model – both not reported in past literature – are expected to improve the fundamental understanding of and optimize heat transfer in polymer AM processes, potentially leading to parts with unique thermal properties, such as high thermal conductivity, anisotropic thermal conductivity as well as spatially-varying thermal conductivity.

2. Experiments

Experiments are carried out to investigate improvement in build direction thermal conductivity through thermal annealing. Next subsections describe various aspects of the experimental approach.

2.1. Sample design and printing

ABS samples are designed to facilitate build-direction thermal conductivity measurement and printed on a Stratasys Fortus 450mc tool. As described in Section 2.3, thermal conductivity measurement through differential heat flux measurement requires two samples of the same cross section but different thicknesses. In this case, two samples of 4 mm and 8 mm thicknesses, and 36 mm by 36 mm cross-section are designed. These dimensions ensure sufficient difference in material thermal resistances of the two samples as well as compatibility with the measurement equipment. CAD drawings of the samples are prepared through SolidWorks and processed in Insight slicing software. The detailed toolpath is then exported as a. cmb file and fed into the control software of the 3D printer. Geometrical parameters of the sample include 0.25 mm layer height, 0.41 mm raster width and 0.25 mm air gap. These parameters are chosen in order to minimize neck formation during the printing process prior to annealing. Raster lines are stacked in the same orientation in all layers. The build direction in the printing process is aligned with the thickness of the samples, so that the build-

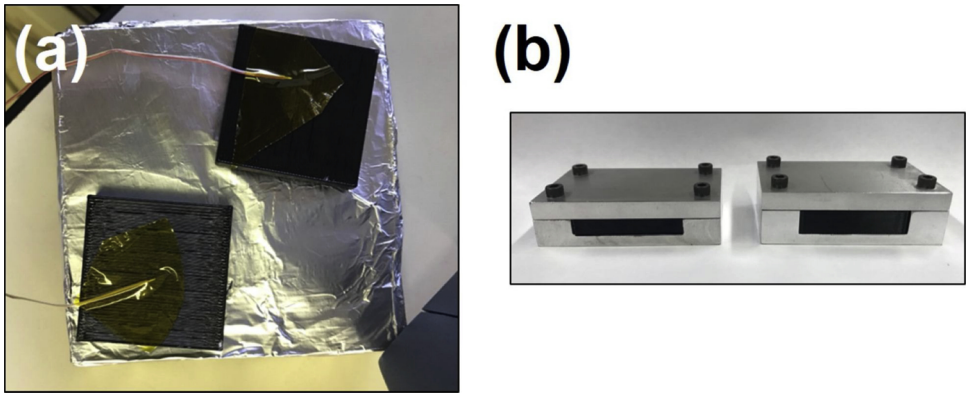

Fig. 1. (a) Picture of a pair of samples for build-direction thermal conductivity measurement; (b) Picture of the sample holder for mounting samples during annealing process.

direction thermal conductivity can be measured in isolation from thermal conductivity in other directions.

Fig. 1(a) shows a picture of a representative pair of samples printed for build-direction thermal conductivity measurement.

2.2. Experimental setup for thermal annealing

All thermal annealing experiments are carried out in a Boekel Scientific high temperature oven. A set of oven calibration tests are carried out in advance of the experiments, in order to account for possible difference between the set temperature and actual temperature of the sample inside the oven. In these experiments, a test sample is placed in the sample holder and kept in a fixed location of the oven. Fig. 1(b) shows a picture of the sample holder used in this work. Temperature of the sample is measured with a T-type thermocouple and the set temperature of the oven is adjusted in order for the sample temperature to reach the desired value. By doing so, oven temperature setting needed for each sample temperature of interest is determined.

In each experiment with an actual sample, the oven is first set to the desired temperature and allowed to reach steady state, as determined by stability of temperature measurement from a thermocouple inside the oven. The test sample, mounted in a sample holder is introduced. After the desired time duration for the annealing experiment has been reached, the oven is switched off and allowed to cool down on its own. This prevents thermal shock to the sample if withdrawn from the oven and exposed abruptly to the relatively cold ambient. Once the oven has cooled down to room temperature, the sample is dismounted from the sample holder. Minor warping of samples is found to occur at corners in some cases, which is corrected by gently filing the corners of the sample on both faces.

A sample holder is designed and fabricated for holding the sample, thereby providing repeatability across multiple experiments. The sample holder is made from aluminum to provide the least temperature variation and thermal resistance around the sample. The bottom plate of the sample holder has a cavity to house the sample, while the top plate covers the sample. A cut is provided to insert a thermocouple to monitor the sample temperature during annealing.

2.3. Experimental setup for thermal conductivity measurements

Fox50 apparatus based on differential heat flux measurement method is used for measuring build direction thermal conductivity of samples before and after thermal annealing. This method is based on measurement of heat flux induced by a fixed temperature difference across the thickness of the sample. Interfacial thermal contact resistance between the sample surface and instrument is eliminated by separately measuring the heat fluxes Q_1 and Q_2 for two samples of different thicknesses L_1 and L_2 subjected to the same temperature difference ΔT. As shown schematically in Fig. 2, the two key thermal resistances that combine in series to form the measured total thermal resistance comprise the material thermal resistance, which is proportional to the sample thickness, and the sample-to-instrument thermal contact resistance, which is assumed to be the same for both samples. This is a reasonable assumption since the surface finish of both samples is the same. The unknown sample-to-instrument thermal contact resistance may be eliminated by subtracting the measured total thermal resistance. The thermal conductivity of the material can be shown to be given by [13,24]

$$k = \frac{Q_1 Q_2 (L_1 - L_2)}{(Q_1 - Q_2)\Delta T} \quad (1)$$

This method has been used extensively for measurement of thermal conductivity in a variety of engineering applications, including for additively manufactured samples [13].

Fig. 3 shows a schematic of the experimental approach, including details of the annealing times and temperatures investigated in this work.

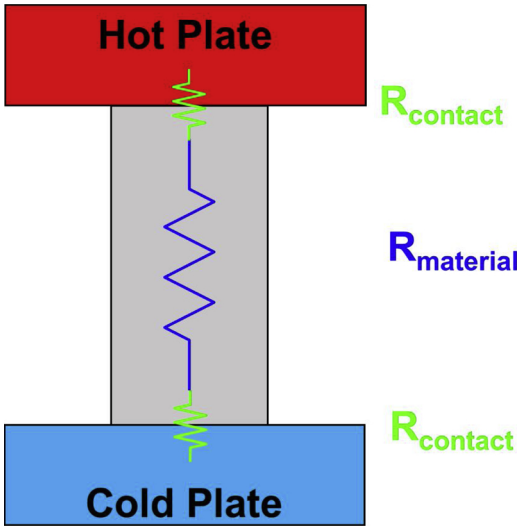

Fig. 2. Schematic of various thermal resistances in the thermal conductivity measurement experiment.

2.4. Cross-section visualization

After annealing and thermal property measurements, samples are cut normal to the raster direction, such that the plane of the cut reveals the cross-section microstructure of filaments. This facilitates quantitative measurement of filament-to-filament necking after annealing. These data play a key role in validating and determining the coefficients of the theoretical model. Since ABS is a thermoplastic material, any attempt to cut it with conventional methods will disrupt the internal structure due to local melting and redistribution of material. Instead, a small notch is made around the sample, which is then soaked in liquid Nitrogen for 1–2 min. This temporarily makes the sample brittle, which can be broken by applying an impact load from a hammer at the notch while the sample is still very cold. It is found that this approach results in a clean cut that does not disrupt the internal filament microstructure of the samples [13,14].

Cross-section images are taken with a MU1000 camera mounted on an AmScope microscope. Neck size is measured from images taken at the same zoom setting. An image of two lines with a spacing of 1 mm captured by the camera is used for calibration and quantification of the magnification. All cross-section images are then taken with the same settings. Each image corresponding to a particular annealing time and temperature is found to have 10–20 visible necks. An average of these neck size measurements is recorded as the neck diameter for that particular annealing experiment.

3. Theoretical modeling

Recent experimental measurements have shown lower thermal conductivity in the build direction compared to the raster direction due to significant thermal contact resistance between layers in the build direction [13]. This section proposes a theoretical model for determining the extent of enhancement in build-direction thermal conductivity when a sample is isothermally exposed to a high temperature T for a time duration t. A relationship between the two key annealing parameters – temperature and time – and neck growth based on Arrhenius kinetics is discussed in Section 3.1. This neck growth is then shown to lead to reduced thermal contact resistance, and hence, increased thermal conductivity in Section 3.2.

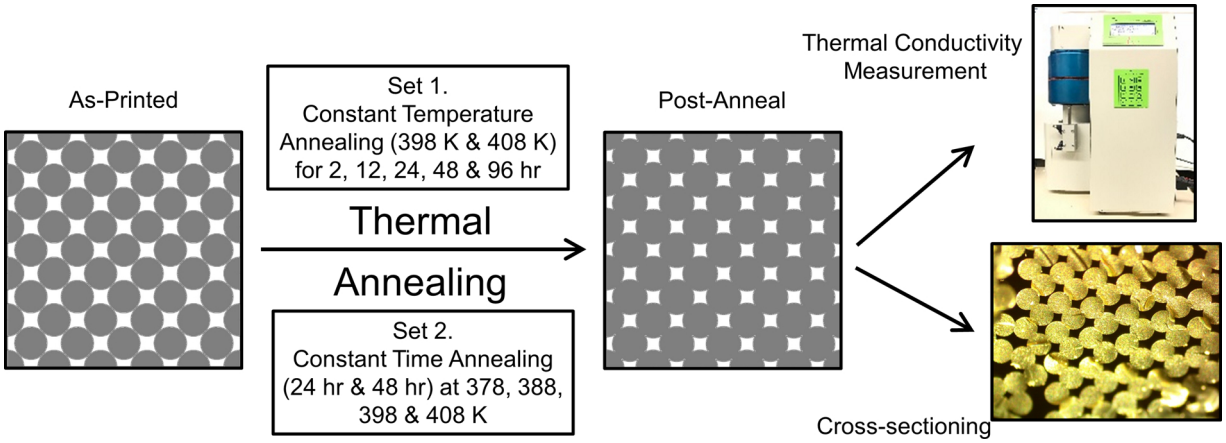

Fig. 3. Schematic of the experimental flow followed in this work, including details of annealing times and temperatures for two sets of annealing experiments.

3.1. Kinetic growth model

Microstructural growth in materials in response to thermal annealing is well known, with extensive experimental data and theoretical models in the past literature. For example, grain growth in crystalline materials occurs when exposed to high temperature for a certain time, and is used routinely for improving properties of traditionally manufactured metal parts [16]. The growth of grains is typically based on Arrhenius kinetics and is modeled by a power law [25,26] of the following form

$$d^n - d_0^n = k_0 \cdot \exp\left(-\frac{E}{RT}\right) \cdot t \tag{2}$$

where d_0 is the initial size, d is the increased size after annealing. E is the activation energy for the neck growth process and R is the universal gas constant. n and k_0 are constants that are typically determined by comparison with experimental data [25,26]. It is proposed that neck growth in polymer AM samples is also characterized by a similar power law. In the present case where neck growth is considered in response to thermal annealing, $d_0 = 0$ since there is no necking initially. This assumption is justified because of significant filament-to-filament gap designed in the printing process. Further, past work shows that thermal penetration into previously deposited layers during the printing of a fresh layer is not strong enough to significantly increase neck size [27].

Thus, in the case of neck growth, Eq. (2) can be written as:

$$d^n = k_0 \cdot \exp\left(-\frac{E}{RT}\right) \cdot t \tag{3}$$

where, in the context of neck growth, d refers to the neck size.

3.2. Heat transfer model

Total thermal resistance in the build direction is the sum of thermal resistances offered by each layer and the total contact resistance between layers [13]. Therefore, thermal conductivity (k_z) in the build direction is given by [13]:

$$\frac{1}{k_z} = \frac{1}{k_{layer}} + \frac{R_C}{h} \tag{4}$$

where k_{layer} is the material thermal conductivity of the filament material, R_C is the thermal contact resistance between the layers and h is the layer height.

Thus, the baseline thermal conductivity prior to thermal annealing, $k_{z,0}$ can be written as:

$$\frac{1}{k_{z,0}} = \frac{1}{k_{layer}} + \frac{R_{C,0}}{h} \tag{5}$$

where $R_{C,0}$ is the baseline thermal contact resistance.

The increase in neck size increases the contact area between filaments, resulting in a reduction in thermal contact resistance between layers. The mathematical relationship between neck size and contact resistance is not known. In this paper, it is proposed that inter-layer thermal contact resistance in the annealed sample is related to the neck size as:

$$R_{C,a} = R_{C,0} - \beta \cdot d^m \tag{6}$$

where β (> 0) and m (> 1) are constants.

Eq. (6) hypothesizes that a larger neck size will reduce thermal contact resistance due to the d^m scaling. Further, because thermal contact resistance is likely to scale with the area of contact between filaments in adjacent layers, the value of m may be expected to be close to 2, since the area of contact scales with the square of the neck size.

Using Eqs. (4) and (6), an expression for thermal conductivity of the annealed sample may be written as:

$$\frac{1}{k_{z,a}} = \frac{1}{k_{layer}} + \frac{R_{C,0}}{h} - \frac{\beta}{h} \cdot d^m \tag{7}$$

Using Eq. (5), this simplifies to

$$\frac{1}{k_{z,a}} = \frac{1}{k_{z,0}} - \frac{\beta}{h} \cdot d^m \tag{8}$$

Eq. (8) is a model that connects microstructure of the annealed part with its thermal conductivity. The neck size d in Eq. (8) is related to the annealing parameters T and t through the kinetic model, Eq. (3). Therefore, by combining the kinetic and heat transfer models, thermal conductivity of the annealed sample can be related to the annealing time (t) and temperature (T) as:

$$\frac{1}{k_{z,a}} = \frac{1}{k_{z,0}} - \frac{\beta}{h} \cdot \left(k_0 \cdot \exp\left(-\frac{E}{RT}\right) \cdot t\right)^{m/n} \tag{9}$$

Eq. (9) is the key result that relates thermal conductivity enhancement with annealing time and temperature. The key assumptions behind this result include Arrhenius based neck growth kinetics, and the scaling of inter-layer thermal contact resistance with d^m. While Eq. (3) connects microstructure with process, Eq. (8) connects the microstructure with resulting thermal properties of the built part. In contrast with well-established experimental and theoretical work on annealing of metal parts, not much literature exists on thermal annealing of AM parts. Therefore, the validity of these assumptions needs to be established based on comparison with experimental data. Specifically, a number of parameters in the theoretical model – m, n, β, k_0 and E – must be determined by fitting experimental data with theoretical equations, and the accuracy of resulting relationships between T, t, d and k_z must be established by comparison with experimental data. These important

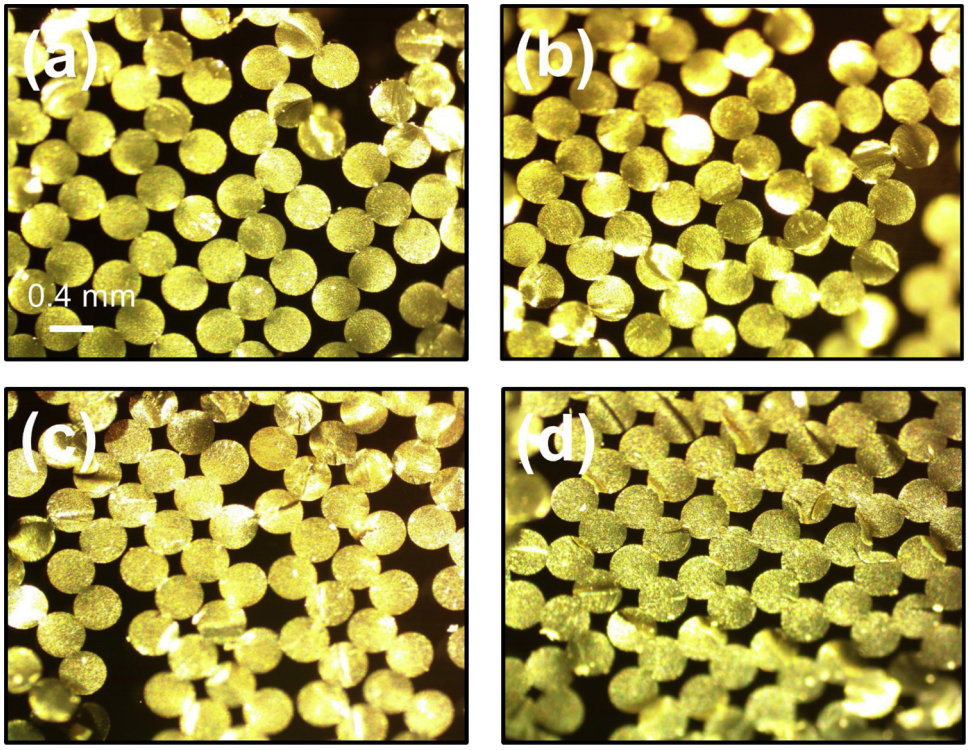

Fig. 4. Cross-section images showing the extent of filament-to-filament necking in four samples annealed at 398 K for different times. (a)–(d) show samples annealed for 12, 24, 48 and 96 h respectively. Note that the build direction for each cross-section image is from bottom to top.

issues are addressed in Section 4.2.

Note that the model proposed in this section is not valid at very high temperatures where other physical processes, such as polymer melting become important, or at very low temperatures close to or lower than the glass transition temperature, where thermally-driven filament deformation is no more significant. There is also an upper limit on possible thermal conductivity enhancement due to annealing, since thermal conductivity of the part clearly can not exceed that of the underlying material.

4. Results and discussion

4.1. Cross-section visualization and neck size measurement

Cross-sections of samples before and after thermal annealing are visualized and the neck size is measured using the technique discussed in Section 2.4. Fig. 4 shows a set of four images of cross-section images from four samples annealed at 125 °C (398 K) for different times, including a baseline sample prior to annealing. Significant progression in neck size is seen as annealing time increases. This increase is central to the theoretical model for annealing-based thermal conductivity enhancement. Note that the build direction for cross-section images shown in Fig. 4 is from bottom to top.

4.2. Parameter extraction from theoretical models

Eq. (3) shows that for constant-temperature annealing experiments, the relationship between d^n and t must be linear. Therefore, the value of n can be determined as that value which results in a linear d^n vs. t plot. In order to examine this in detail, annealing experiments as described in Section 2.2 are carried out at 398 K for 12, 24, 48 and 96 h. In each case, the neck size d is determined using the process described in Section 2.4. d^n vs. t plots are generated for multiple values of n. Through least squares fitting, the most linear relationship between d^n and t is found to occur for a value of $n = 2.6$. This best fit is shown in Fig. 5,

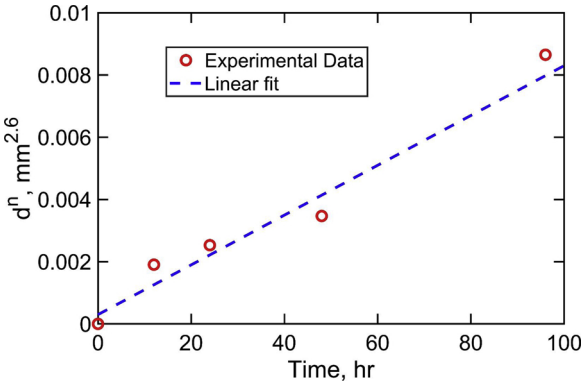

Fig. 5. Plot of d^n and t for $n = 2.6$, based on measurement of neck sizes of samples annealed at 398 K for different times. A value of $n = 2.6$ results in the most linear fit, as predicted by the power law in the kinetic model.

which shows an excellent linear fit between $d^{2.6}$ and t. The value of n determined in this manner is in the same range as the power exponent for grain growth models [25, 26], even though the material systems are quite different

Values of the other kinetic parameters – E and k_0 – are obtained next. In order to do so, experimental data on neck size as a function of annealing temperature from experiments at constant annealing time are used. Taking logarithm of Eq. (3) results in:

$$ln(d) = -\frac{E}{nRT} + \frac{1}{n}\bullet \ln(k_0) + \frac{1}{n}\bullet ln(t) \tag{10}$$

which shows that for constant-time annealing experiments, a plot of ln (d) vs. $1/T$ is expected to be linear. The slope and intercept of this plot is given by $-E/nR$ and $\ln(k_0 t)/n$, respectively, from where E and k_0 can be determined, since n is already known, d has been measured, and t and R are known constants. Fig. 6 shows a ln(d) vs. $1/T$ plot based on experimental data for a constant time $t = 24$ h and temperatures of 378 K,

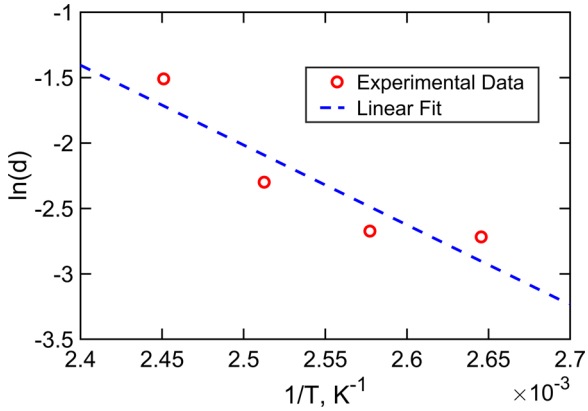

Fig. 6. Plot of ln(d) vs. $1/T$ based on experimental data for a constant time $t = 24$ h. Slope and intercept of this plot facilitate determination of kinetics parameters β and E.

388 K, 398 K and 408 K. Fig. 6 shows good linearity between the two. A slope of -6103.9 K and an intercept of 13.244 are obtained, based on which, the values of E and k_0 are found to be 131.944 kJ/mol and 3.75×10^{13} mm$^{2.6}$/hr respectively.

Finally, the values of m and β – parameters that govern the relationship between microstructure and thermal properties – are determined by plotting $1/k_{z,0} - 1/k_{z,a}$ as a function of d^m. This utilizes measurements of neck size as described in Section 2.4 and of thermal conductivity as described in Section 2.3. Experimental data for annealing temperatures of 388 K, 398 K and 408 K at a constant annealing time of 24 h are utilized. The value of m is determined to be the value that results in linear relationship between d^m and $1/k_{z,0} - 1/k_{z,a}$. Further, the slope of this relationship can be used to determine β. The best linear fit is found for a value of $m = 2.0$, and is shown in Fig. 7. Based on the slope of the best fit line in Fig. 7, determined to be 91.95 K/(W·m), and a layer height of $h = 0.4$ mm based on print settings, the value of β is calculated to be 36.78 K/W. The value of $m = 2.0$ obtained from experimental data analysis is consistent with the expectation that the inter-layer contact resistance must scale with the contact area, which in turn scales with the square of the neck size, as discussed in Section 2.2.

In this manner, experimental data at different annealing temperatures and times are utilized to validate the theoretical models and determine the key parameters involved in the models. Once these parameters are known, it is possible to theoretically predict the enhancement in thermal conductivity for any annealing temperature

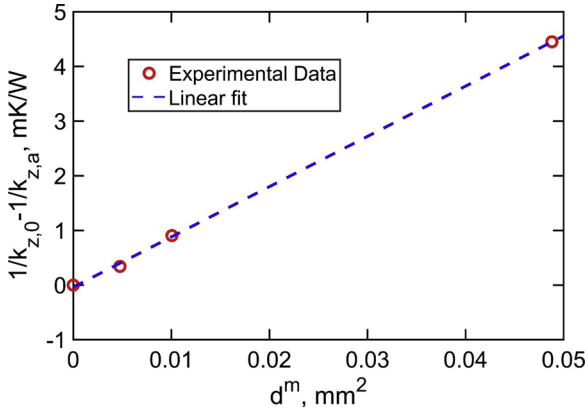

Fig. 7. Plot of $1/k_{z,0} - 1/k_{z,a}$ as a function of d^m for $m = 2.0$, which results in the most linear fit, as predicted by the heat transfer model. Thermal conductivity and neck size measurements are based on experimental procedures described in Section 2.

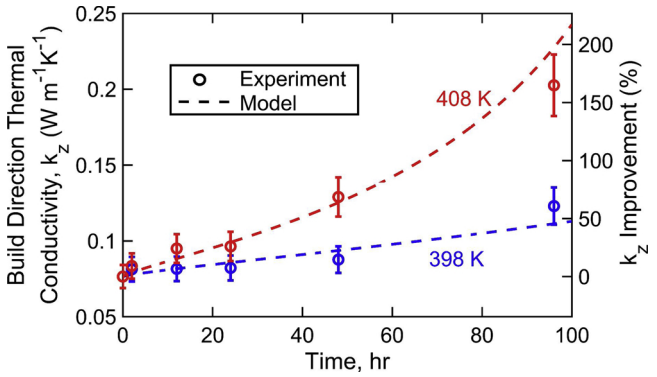

Fig. 8. Comparison of measured thermal conductivity as a function of annealing time for two different oven temperatures – 398 K and 408 K – with prediction from the theoretical model.

and time. Note that the model parameters determined in this sub-section are specific to the filament material used here, and possibly to other process parameters as well, such as filament size, dispense temperature, as these parameters all affect the nature of bonding between adjacent filaments. Therefore, for a different material, or a different set of process parameters, these parameters may need to be determined again.

4.3. Comparison of experimental data with theoretical model

Based on model parameters determined in Section 4.1, experimental measurements of thermal conductivity as a function of annealing temperature and time are compared with the theoretical model. Fig. 8 plots measured post-annealing thermal conductivity as a function of annealing time for two different oven temperatures – 398 K and 408 K. At each data point shown in Fig. 8, the sample is annealed using the process described in Section 2.2, followed by thermal conductivity measurement as described in Section 2.3. These data show significant enhancement in thermal conductivity with increasing time. While thermal conductivity enhancement is somewhat minor at small times, the rate of improvement goes up non-linearly at large times. As expected, thermal conductivity enhancement is greater for experiments at 408 K than at 398 K due to the higher temperature. Fig. 8 also shows corresponding predictions of thermal conductivity enhancement based on the theoretical model, specifically Eq. 9, using the model parameters determined in Section 4.2. Fig. 8 shows that the theoretical model accurately captures the trend in experiments, for data at both annealing temperatures, with good agreement with experimental measurements.

For further comparison of experimental data with the theoretical model, measured thermal conductivity values are plotted in Fig. 9 as a function of annealing temperature for experiments carried out for the same time duration. Two sets of data – at 24 h and 48 h – are shown. Similar to Fig. 8, this plot also shows increasing thermal conductivity with increasing annealing temperature, and greater thermal conductivity for the 48 h data compared to 24 h data, for any given annealing temperature. The gap between thermal conductivity for the two sets of data is particularly significant at high annealing temperature, such as 408 K, showing that in order to obtain the same thermal conductivity enhancement, the annealing time can be significantly reduced by relatively small increase in annealing temperature. Theoretically, this happens because, as shown in Eq. (2), while d^m increases linearly with t, the dependence on T is much stronger due to its occurrence in the non-linear, exponential term.

It is instructive to compare the thermal conductivity enhancement reported here with enhancement in fracture toughness reported by Hart, et al. [17] under similar annealing conditions. For example, Fig. 8 shows over 150% enhancement in thermal conductivity for annealing at 408 K for 96 h. For similar conditions, Hart, et al. [17] reported around

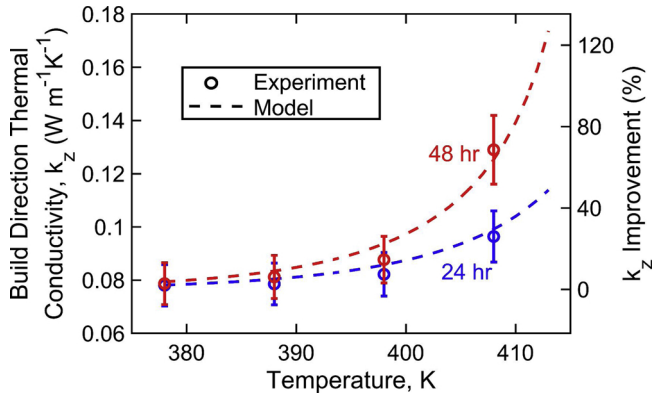

Fig. 9. Comparison of measured thermal conductivity as a function of annealing temperature for two different anneal times – 24 h and 48 h – with prediction from the theoretical model.

2700% improvement in fracture toughness. As such, thermal conductivity of polymers does not vary over such a large range, as does a mechanical property such as fracture toughness. A 150% increase in thermal conductivity itself brings the value close to the baseline value of the filament material itself [28], which clearly is an upper limit for the thermal conductivity. Further, note that while the theoretical model for fracture toughness in Hart, et al. [17] predicts an exponential dependence on time, thermal conductivity is expected to increase much less with time, as shown in Eq. (9).

Uncertainty in thermal conductivity measurement is the key source of measurement uncertainty in data shown in Figs. 8 and 9. Other sources of uncertainty include uncertainty in temperature measurement, sample thickness measurement, etc.

4.4. Annealing process design space

Based on the experimentally validated analytical model discussed in Sections 4.2 and 4.3, the thermal design space for the annealing process can be explored in order to predict design parameters that result in desired thermal conductivity enhancement. Design of experiments based on predictions from the analytical model is particularly important because the annealing time must be minimized for increasing throughput, and also because there are several restrictions on the temperature range.

The two key process parameters of relevance for thermal annealing include annealing temperature T and annealing time t. Fig. 10 presents a colorplot of theoretically predicted thermal conductivity enhancement as a function of T and t. This plot offers several interesting insights. In general, the higher the value of T and/or t, the greater is the thermal conductivity enhancement. Specifically, the dependence on T is highly non-linear, with negligible improvement at low temperatures, regardless of the annealing time, and dramatically greater thermal conductivity improvement at greater times. There exist a number of (T,t) pairs that lead to the same thermal conductivity enhancement. As an example, Fig. 10 shows multiple curves along each of which, all (T,t) points result in the same thermal conductivity enhancement. This indicates that there are several process design choices for the same eventual outcome. However, this is constrained by several other considerations. For example, while increasing temperature does offer the convenience of reduced annealing time for achieving the same outcome in terms of thermal conductivity enhancement, too high a temperature results in softening and mechanical distortion of the sample. On the other hand, annealing at low temperature for a very long time is unrealistic as it reduces throughput. Further, as discussed Section 4.5, a sample takes some time to equilibrate to the oven temperature after being inserted, which could be several hours depending on the sample size. In between all of these conflicting considerations, one must determine an optimal strategy for obtaining the desired goal of thermal conductivity enhancement.

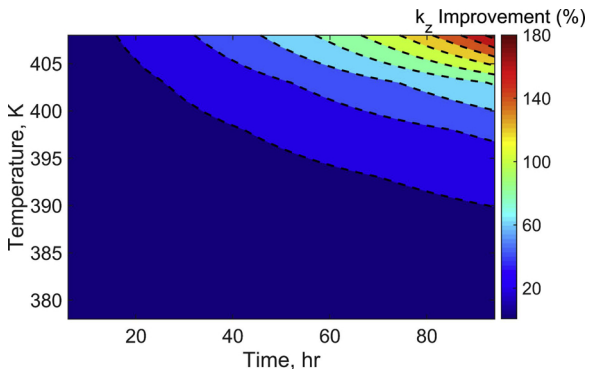

Fig. 10. Colorplot of predicted post-annealing thermal conductivity in the (T,t) space.

4.5. Non-isothermal annealing

The analytical model presented in Section 3 assumes that the sample anneals in isothermal conditions corresponding to the oven temperature. However, depending on the size of the sample, it is possible that the sample might take a significant amount of time to reach close to the oven temperature. If this time is comparable to the total anneal time, then annealing occurs in a non-isothermal manner, wherein the sample temperature itself changes with time. From a heat transfer perspective, the time taken for the sample to reach close to the oven temperature depends on the thermal mass of the sample and rate of convective heat transfer from the oven ambient to the sample. When the Biot number is reasonably small, the sample may be assumed to be a lumped thermal mass [29], so that the thermal time constant is given by $\frac{\rho C_p V}{hA}$, where ρ, C_p, V, h, and A are density, specific heat, volume, convective heat transfer coefficient and surface area respectively. Based on the geometry of samples used in these experiments, and assuming free convection conditions inside the oven, the Biot number for present experiments is found to be 1.2–1.8, which is not small. As a result, a simple lumped thermal mass assumption is not valid, and the thermal history of the sample during oven acclimatization must be determined through alternative approaches such as a finite-element simulation. Fig. 11 plots temperature as a function of time for two samples of different sizes during oven acclimatization, starting from room temperature and up to the oven temperature of 135 °C. Fig. 11 shows that the time taken for the sample to reach oven temperature is a function of the sample size. Isothermal conditions during annealing may not be

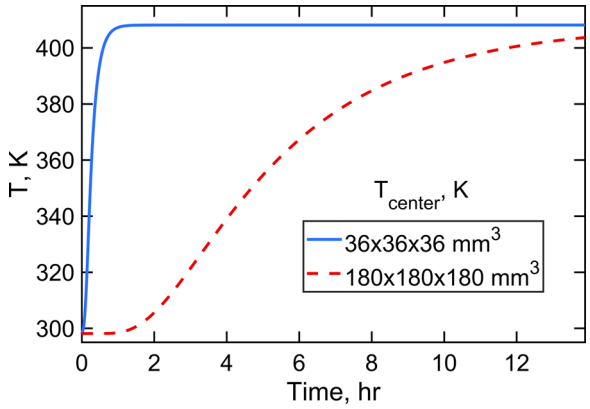

Fig. 11. Temperature as a function of time after inserting a sample in an oven set at 135 °C for annealing. Plots are shown for two samples of different sizes.

assumed for relatively large samples.

The analytical model for thermal conductivity enhancement presented in Section 2 can be extended to account for non-isothermal conditions. The neck size d, which Eq. (3) determines based on a constant temperature assumption must now consider changes in temperature with time, and therefore,

$$d^n = \int_0^t k_0 \cdot exp\left(-\frac{E}{RT(\tau)}\right) d\tau \tag{11}$$

so that the total enhancement in thermal conductivity over time t is given by a generalization of Eq. (9)

$$\frac{1}{k_{z,a}} = \frac{1}{k_{z,0}} - \frac{\beta}{h} \cdot \left(\int_0^t k_0 \cdot exp\left(-\frac{E}{RT(\tau)}\right) d\tau \right)^{m/n} \tag{12}$$

5. Conclusions

Thermal annealing is a promising post-process technique for improving properties of polymer extrusion based parts. While enhancement in mechanical properties has been demonstrated in the past, this work shows that a similar effect exists for thermal conductivity, which is a key property governing the rate of flow of heat. The annealing-driven enhancement reported here restores the thermal conductivity of the part to nearly the thermal conductivity of the underlying material. The theoretical model presented here provides key insights into the nature of annealing-driven enhancement, and is in good agreement with experimental data. Optimal design of the annealing process based on results discussed here may help improve thermal properties of polymer extrusion based parts, and facilitate the use of such parts in applications where significant heat loads are expected.

Acknowledgments

Authors would like to acknowledge the support of Rice University's Biomaterials Laboratory.

References

[1] D. Dimitrov, K. Schreve, N. de Beer, Advances in three dimensional printing – state of the art and future perspectives, Rapid Prototyp. J. 12 (2006) 136–147.
[2] D.T. Pham, R.S. Gault, A comparison of rapid prototyping technologies, Int. J. Mach. Tools Manuf. 38 (1998) 1257–1287.
[3] B.N. Turner, R. Strong, S.A. Gold, A review of melt extrusion additive manufacturing processes: I. Process design and modeling, Rapid Prototyp. J. 20 (2014) 192–204.
[4] I. Gibson, D. Rosen, B. Stucker, Additive Manufacturing Technologies: 3D Printing, Rapid Prototyping, and Direct Digital Manufacturing, Springer, 2014.
[5] J. Kotlinski, Mechanical properties of commercial rapid prototyping materials, Rapid Prototyp. J. 20 (2014) 499–510.
[6] T. Osborn, E. Zhou, Gerzeski R, D. Mollenhauer, G.P. Tandon, T.J. Whitney, E.V. Iarve, Experimental and theoretical evaluation of stiffness properties of fused deposition modeling parts, American Society of Composites – 30th Technical Conference, (2015).
[7] S. Sheth, R.M. Taylor, A. Adluru, Numerical investigation of stiffness properties of FDM parts as a function of raster orientation, Proceedings of the Annual Solid Freeform Fabrication Symposium (2017).
[8] S.H. Ahn, M. Montero, D. Odell, S. Roundy, P.K. Wright, Anisotropic material properties of fused deposition modeling ABS, Rapid Prototyp. J. 8 (2002) 248–257.
[9] A. Bellini, S. Güçeri, Mechanical characterization of parts fabricated using fused deposition modeling, Rapid Prototyp. J. 9 (2003) 252–264.
[10] J. Lee, A. Huang, Fatigue analysis of FDM materials, Rapid Prototyp. J. 19 (2013) 291–299.
[11] H. Zhang, Characterization of Tensile, Creep, and Fatigue Properties of 3D Printed Acrylonitrile Butadiene Styrene, Purdue University Indianapolis, Doctoral Dissertation, 2016.
[12] K.P. Motaparti, Effect of Build Parameters on Mechanical Properties of Ultem 9085 Parts by Fused Deposition Modeling, Master's Thesis, Missouri University of Science and Technology, 2016.
[13] H. Prajapati, D. Ravoori, R.L. Woods, A. Jain, Measurement of anisotropic thermal conductivity and inter-layer thermal contact resistance in polymer fused deposition modeling (FDM), Addit. Manuf. 21 (2018) 84–90.
[14] D. Ravoori, L. Alba, H. Prajapati, A. Jain, Investigation of process-structure-property relationships in polymer extrusion based additive manufacturing through in situ high speed imaging and thermal conductivity measurements, Addit. Manuf. 23 (2018) 132–139.
[15] T. Sonsalla, A.L. Moore, W.J. Meng, A.D. Radadia, L. Weiss, 3-D printer settings effects on the thermal conductivity of acrylonitrile butadiene styrene, Polym. Test. 70 (2018) 389–395.
[16] W.D. Callister Jr., D.G. Rethwisch, Fundamentals of Materials Science and Engineering: an Integrated Approach, John Wiley & Sons, 2012.
[17] K.R. Hart, R.M. Dunn, J.M. Sietins, C.M.H. Mock, M.E. Mackay, E.D. Wetzel, Increased fracture toughness of additively manufactured amorphous thermoplastics via thermal annealing, Polymer 144 (2018) 192–204.
[18] M.D. Wolkowicz, S.K. Gaggar, Effect of thermal aging on impact strength acrylonitrile-butadiene-styrene (ABS) terpolymer, Polym. Eng. Sci. 21 (1981) 571–575.
[19] Y.H. Kim, R.P. Wool, A theory of healing at a polymer-polymer interface, Macromolecules 16 (1983) 1115–1120.
[20] P.G. de Gennes, Reptation of a polymer chain in the presence of fixed obstacles, J. Chem. Phys. 55 (1971) 572–579.
[21] S. Mazur, Coalescence of polymer particles, Polymer Powder Technology, John Wiley & Sons, New York, 1995.
[22] C. Bellehumeur, L. Li, Q. Sun, P. Gu, Modeling of bond formation between polymer filaments in the fused deposition modeling process, J. Manuf. Process. 6 (2004) 170–178.
[23] O. Pokluda, C. Bellehumeur, J. Vlachopoulos, Modification of Frenkel's model for sintering, Aiche J. 43 (1997) 3253–3256.
[24] V. Vishwakarma, C. Waghela, Z. Wei, R. Prasher, S.C. Nagpure, J. Li, F. Liu, C. Daniel, A. Jain, Heat transfer enhancement in a Lithium-ion cell through improved material-level thermal transport, J. Power Sources 300 (2015) 123–131.
[25] M.A. Guitar, K. Woll, E. Ramos-Moore, F. Mücklich, Study of grain growth and thermal stability of nanocrystalline RuAl thin films deposited by magnetron sputtering, Thin Solid Films 527 (2013) 1–8.
[26] X. Wang, L. Hu, K. Liu, Y. Zhang, Grain growth kinetics of bulk AZ31 magnesium alloy by hot pressing, J. Alloys. Compd. 527 (2012) 193–196.
[27] J.E. Seppala, K.D. Migler, Infrared thermography of welding zones produced by polymerextrusion additive manufacturing, Addit. Manuf. 12 (2016) 71–76.
[28] www.professionalplastics.com/professionalplastics/ThermalPropertiesofPlasticMaterials.pdf accessed 10/26/2018.
[29] F.P. Incropera, D.P. DeWitt, T.L. Bergman, A.S. Levine, Introduction to Heat Transfer, 5th ed., John Wiley & Sons, 2006.